Frozen Leg Operation of a Three-Phase Dual Active Bridge DC/DC Converter at Light Loads

Saeid Haghbin*, Frede Blaabjerg†, Farzad Yazdani‡ and Amir Sajjad Bahman†
*Electric Power Engineering, Chalmers University of Technology, Gothenburg, 412 96 Sweden
Email: saeid.haghbin@elbind.se
†Department of Energy Technology, Aalborg University, Aalborg, 9220, Denmark
Emails: fbl@et.aau.dk and asb@et.aau.dk
‡ Department of Electrical Engineering, Sharif University of Technology, Tehran, Iran
email: yazdani_farzad@ee.sharif.edu

***Abstract*—A three-phase dual active bridge (DAB) converter is designed and constructed as the DC/DC stage of a $50\ kW$ fast charger station. Recently introduced $300A$ SiC power modules and drivers are utilized in the converter to obtain a high efficiency. Each module has two interconnected switches with anti-parallel diodes resembling a converter leg. It is observed that the driver halts the module operation as a result of protective actions such as over-current, gate under-voltage, or gate over-voltage. In such case the module operates as a leg with two diodes until an external hardware signal resets the driver. The aim of this paper is to provide analysis, simulation and experiments for a three-phase DAB converter after a frozen leg condition in the secondary side of the converter and at light loads. The results show that this fault mode is non-destructive and it is possible to continue the operation by adjusting the controller and over-sizing the semiconductors.**

I. Introduction

Fast charger station is one of the key elements towards more electric transport systems [1], [2]. To achieve a smaller size of the chargers, a higher operating frequency is intended but the magnetic and semiconductor losses increase. Devices can operate in higher temperatures but thermal stresses reduces the component and system reliability [3]. Hence, the reliability aspects including different fault analysis are important for further enhancement of power electronic systems.

DAB topology is one of the interesting topologies for DC/DC conversion, especially the three-phase variation for high power applications [4]–[6]. In high power applications, SiC modules and Nanocrystalline magnetic materials can be used to achieve a higher efficiency and power density. Fig. 1 shows the power stage of the three-phase DAB. The selected polarities for the voltages, currents and different points of the circuit are defined in this figure too. Two active three-phase bridges generate three-phase voltages towards the high-frequency transformer. The transformer inductances and inverter voltages determine the direction and amount of the power flow. There are different methods to control the power transfer in which the phase-shift control is one of the widely used techniques for this bidirectional topology [7] and it is selected in this work. It is assumed that the transformer has a $Y-Y$ configuration where the star points are denoted as N_1 and N_2 for the primary and secondary sides, subsequently.

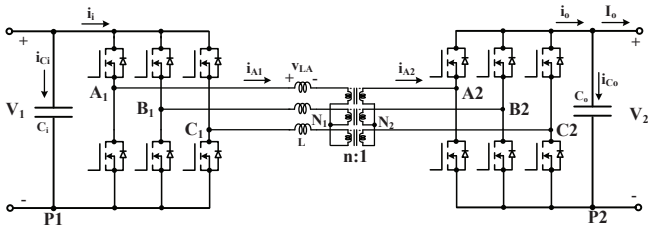

Fig. 1. Equivalent circuit of three-hase DAB converter used in the charger.

A 50 kW prototype for charging applications is constructed utilizing SiC-based 300 A/1200 V modules and related drivers from CREE to reduce the size. The power modules are CAS300M12BM2 and the drivers are PT62SCMD12. This 300 A/1200 V SiC power module has two switches in series to be used as a leg in the converter. Anti-parallel diodes are included in the module also. The gate driver is using an isolating scheme with some protection features. The driver protects the upper and lower switches in the module for the drain over-current and the gate power supply under-voltage and over-voltage.

Reliability is an important aspect of power electronics converters. There are different failure scenarios demands a comprehensive investigation and analysis which failure mode and effect analysis (FMEA) is one tool for a systematic approach for reliability assessment [8]–[12].

For the utilized power modules and drivers, it is observed that the driver halts the module operation when it is subjected to a fault. In this case, the driver re-activates the module after a hardware reset; during this fault mode, the antiparallel diodes are still operative (assuming that they are healthy).

The aim of this paper is to demonstrate converter operation in steady state after a halt in a leg, as a result of the driver protection action. In this case, the converter can continue the operation but with a reduced power level. The fault mode can be detected by monitoring and conditioning of the transformer currents; the transformer currents operate in an unbalanced mode. Moreover, the reduced power transfer capability of the converter is investigated and a fault strategy is proposed in order to increase the power transfer level. Simulation and

978-1-5386-1180-7/18/$31.00 ©2018 IEEE

experimental results are provided to verify the analysis.

It is assumed that the converter is operating in light loads. The converter in high power areas behave differently which is under consideration in a separate work.

II. OPERATION OF THE DAB CONVERTER IN HEALTHY MODE

Fig. 1 shows the topology of a a three-phase DAB where the energy storage inductors of the circuit, L, can be the transformer leakage inductances or external inductors. To analyse the converter, a lossless model of the transformer is used without considering the magnetizing inductances.

The control of the converter is performed via controlling the gate signals of the bridges in the primary and secondary sides. The phase-shift between the primary and secondary determines the direction and magnitude of the power flow. Fig. 2 shows important waveforms of the converter from the gate command to the transformer waveforms in the primary and secondary sides.

The phase-shift angle φ, the input voltage V_1, the output voltage V_2, the transformer primary to secondary turns ratio n, the switching frequency f and series inductance L determine the power transfer as

$$P_{nom} = \frac{n\ V_1 V_2}{\omega L}\varphi\ (\frac{2}{3} - \frac{\varphi}{2\pi}) \tag{1}$$

where $\omega = 2\pi f$ is the angular frequency in rad/s. If the input voltage is equal to the referred output voltage to the primary, i.e. $V_1 = nV_2$, this equation can be written as

$$P_{nom} = \frac{V_1^2}{\omega L}\varphi\ (\frac{2}{3} - \frac{\varphi}{2\pi}). \tag{2}$$

To analyse the converter operation, firstly the inverter output voltages to the negative dc bus, V_{X1P1}, are calculated where X is either A, B or C. Then the transformer voltages to the star points, V_{X1N1}, are calculated. The transformer voltages and the inverter voltages are used to calculate the inductor voltages. Consequently, one can determine the inductor currents. By multiplication of the inductor currents and transformer voltages, it is possible to determine the power. This is the main procedure to analyse the converter in a normal operation.

Now assume that V_{C2P2} is slightly changed. For example, it is turned on after a delay or turned on earlier than is planned. This results in a change in the voltage waveforms in the transformer voltages V_{X2N2}. The new waveforms can be calculated very similar to those shown in Fig. 2.

In case where leg C in the secondary is frozen, V_{C2P2} is deviated from its original shape. Depending on which body diode is conducting, this voltage can be determined. However, to perform an analysis for this case, the same procedure is followed, but with another voltage profile of V_{C2P2}. The inductor voltages and currents are calculated for this case and consequently the power is calculated, which is presented in the next section.

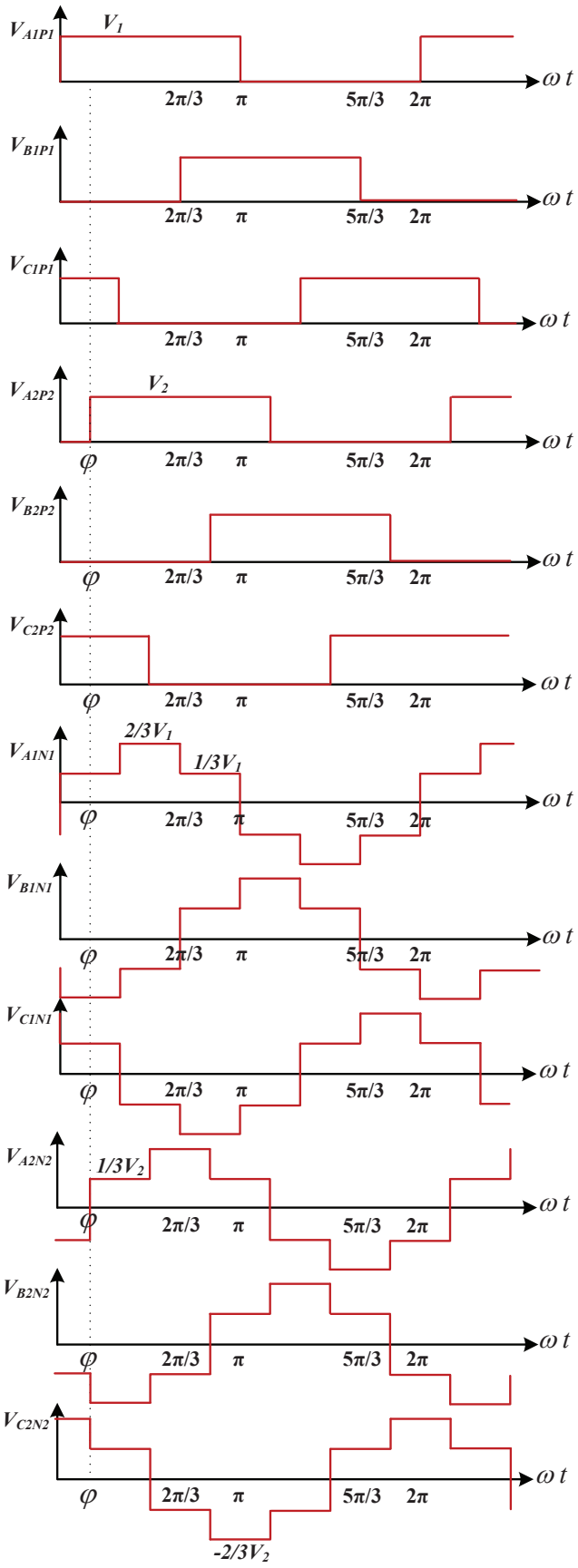

Fig. 2. Ideal waveforms of a three-phase DAB converter.

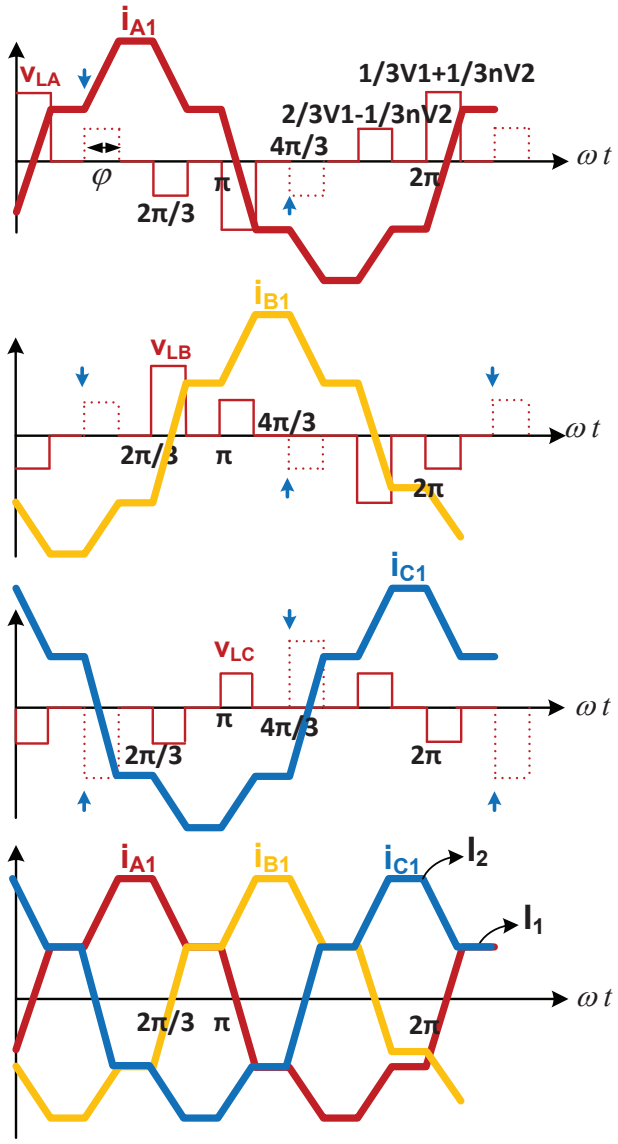

Fig. 3. The inductor waveforms in a three-phase DAB converter.

III. OPERATION OF THE DAB CONVERTER AFTER HALT IN ONE MODULE

The analysis of the converter when leg C in the secondary size is frozen is presented in this section. The inductor waveforms, three-phase voltages and currents, are shown in Fig. 3 in a normal operating condition. The waveforms are for the condition which $V_1 = nV_2$. This case is easier for analysis and holds through the rest of the paper. One part of the inductor voltage is shown by a dashed line and the arrow shows the point of deviation from the original waveform. For frozen leg C, this part of the inductor voltage is affected. This is resulted from basic waveforms of the converter shown in Fig. 2. However, the whole non-linear circuit including the diodes shall be solved to reach an accurate solution.

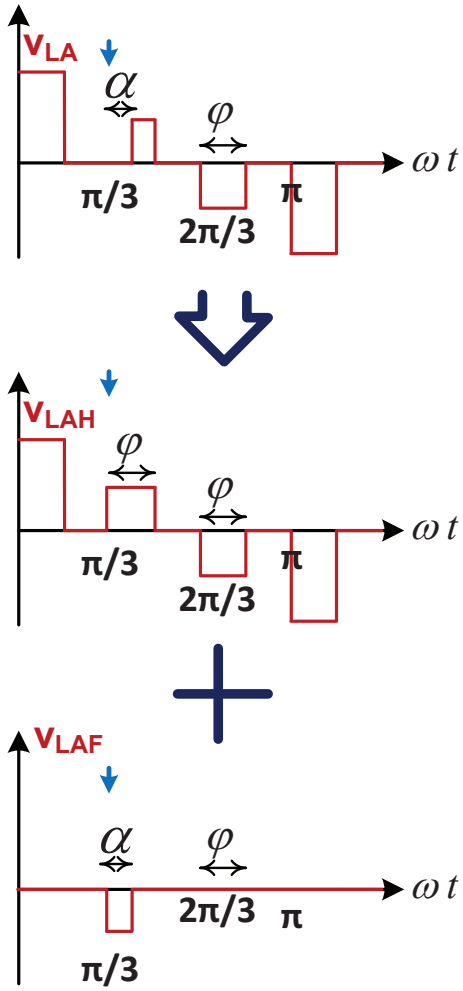

Fig. 4. Decomposition of the inductor voltage for the analysis.

A. Inductor Waveforms Decomposition to Analyse the Frozen Leg Condition

The width of the dashed-line in the inductor voltage is φ. This is the normal width in a normal operation. It is assumed that some part of this pulse is changed to zero as a result of a frozen leg. Hence, it is assumed that the width of α is changed to zero in the frozen leg condition. Angle α is an arbitrary small angle that can be determined in a certain operating condition of the converter. Simulation and experiments are presented later on validation of this assumption. Consequently, the idea is to solve the circuit when the inductor voltage is deviated from its normal operation. In this case the change is that one piece of the inductor voltage in the beginning of the dashed-line area with a width of α is zero.

If α is small, it is possible to use superposition to solve the circuit. It is assumed that the circuit parameters and load conditions are such that the superposition is valid, as is shown in simulations and experiments. Fig. 4 shows the procedure of decomposing the circuit. The width of α is considered as an

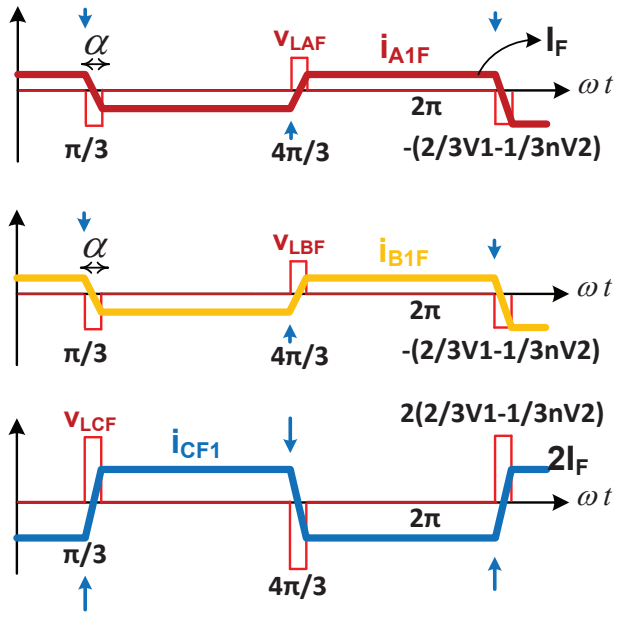

Fig. 5. The indutor waveforms for a decompoed negative voltage pulse.

addition of the original voltage and a negative voltage. In this way, the current can be calculated as the sum of the normal current and the current resulted by a negative pulse with width of α.

For a normal operation of DAB converter, the analysis is not shown here and one can refer to references. For the inductors with a negative voltage pulse, it is possible to solve the circuit to find the current and later on the resulted power. Fig. 5 shows the voltages and currents waveforms as a deviation from normal operation. Phase A and B have similar waveforms while phase C has twice negative value of the current and voltage (sum of three-phase is zero). Note that this waveforms are added to the normal waveforms and can be interpreted as unsymmetrical components.

In steady state condition and considering inductor flux-balance, the value of the inductor current can be calculated as

$$I_F = \frac{V_1 \alpha}{6\omega L} \tag{3}$$

where I_F is the peak current of the inductor and α is the width of voltage pulse in radian.

B. Power Transfer Calculation for the Decomposed Fault Current

In this section, detailed calculations of the transferred power after freezing leg C in the secondary side is presented. For the decomposed fault waveform, the inductor currents and transformer voltages are multiplied and averaged over a half cycle, for each phase. The total power is the addition of the power in normal operation mode and the calculated power for the decomposed waveform (negative pulse of the inductor).

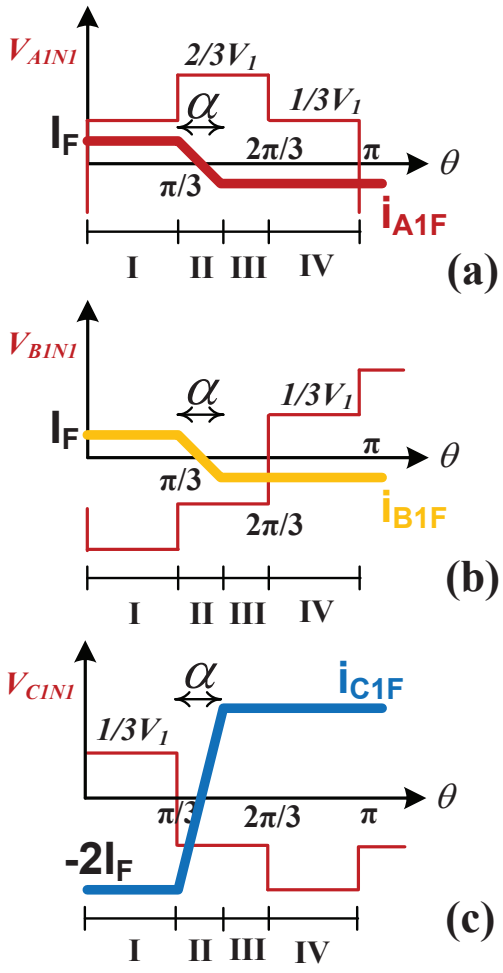

Fig. 6. The transformer waveforms in the primary side after leg C has been frozen.

The analysis is based on the following assumptions: the input/output voltages are equal to the transformer turns ratio, there is no dead-time, the maximum value of the phase shift is 60^o, and the components are ideal. Hence, a slight deviation from the measurement and theoretical values are expected.

Fig. 6.a shows the transformer current and voltage for the phase A. A half cycle is divided into four intervals which the power is calculated for each interval and then it is averaged over a half period to calculate the average power as

$$\begin{aligned} P_{AD} =& \frac{1}{\pi}(P_{ADI} + P_{ADII} + P_{ADIII} + P_{ADIV}) = \\ & \frac{1}{\pi}\int_0^{\pi} V_{A1N1}(\theta) i_{A1}(\theta) d\theta. \end{aligned} \tag{4}$$

For each interval, the power is calculated as

$$P_{ADI} = \frac{1}{3} V_1 I_F \ \pi/3 \tag{5}$$

$$P_{ADII} = 0 \tag{6}$$

$$P_{ADIII} = -\frac{2}{3}V_1 I_F\ (\pi/3 - \alpha) \tag{7}$$

$$P_{ADIV} = -\frac{1}{3}V_1 I_F\ \pi/3. \tag{8}$$

The average power value of the phase A can be calculated as

$$P_{AD} = -\frac{2}{3}V_1 I_F(\frac{1}{3} - \frac{\alpha}{\pi}). \tag{9}$$

The same approach can be used to calculate the power for the phase B and C. For the phase B, the waveforms are shown in Fig. 6.b. A half cycle is divided into four intervals and the average power is

$$P_{BD} = \frac{1}{\pi}(P_{BDI} + P_{BDII} + P_{BDIII} + P_{BDIV}) = \frac{1}{\pi}\int_0^{\pi} V_{B1N1}(\theta) i_{B1}(\theta) d\theta. \tag{10}$$

For each interval, the power is calculated as

$$P_{BDI} = -\frac{2}{3}V_1 I_F\ \pi/3 \tag{11}$$

$$P_{BDII} = 0 \tag{12}$$

$$P_{BDIII} = -\frac{1}{3}V_1 I_F\ (\pi/3 - \alpha) \tag{13}$$

$$P_{BDIV} = -\frac{1}{3}V_1 I_F\ \pi/3. \tag{14}$$

The average power value of the phase B can be calculated as

$$P_{BD} = -\frac{4}{9}V_1 I_F + \frac{1}{3}V_1 I_F\ \alpha/\pi. \tag{15}$$

For phase C, as is shown in Fig. 6.c, four intervals are considered. The average power over a half cycle is

$$P_{CD} = \frac{1}{\pi}(P_{CDI} + P_{CDII} + P_{CDIII} + P_{CDIV}) = \frac{1}{\pi}\int_0^{\pi} V_{C1N1}(\theta) i_{C1}(\theta) d\theta. \tag{16}$$

For each interval, the power is calculated as

$$P_{CDI} = -\frac{1}{3}V_1 I_F\ \pi/3 \tag{17}$$

$$P_{CDII} = 0 \tag{18}$$

$$P_{CDIII} = -\frac{1}{3}V_1\ 2I_F\ (\pi/3 - \alpha) \tag{19}$$

$$P_{CDIV} = -\frac{2}{3}V_1\ 2I_F\ \pi/3 \tag{20}$$

The average power of phase C can be calculated as

$$P_{CD} = -\frac{8}{9}V_1 I_F + \frac{2}{3}V_1 I_F\ \alpha/\pi. \tag{21}$$

Consequently, utilizing (9), (15) and (21), the total average power for the negative pulse component of the waveform in a frozen leg condition, P_{tD}, is

$$P_{tD} = -\frac{14}{9}V_1 I_F + \frac{5}{3}V_1 I_F\ \alpha/\pi. \tag{22}$$

The total power in a frozen leg condition, P_{tF}, is

$$P_{tF} = P_{tD} + P_{nom} \tag{23}$$

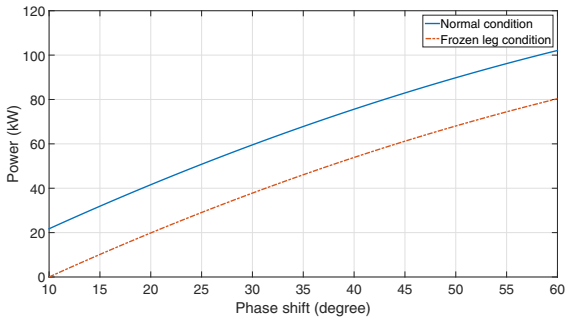

Fig. 7. The converter power in a normal operating condition and a frozen leg mode.

where P_{tD} and P_{nom} are calculated in (2) and (22), subsequently.

Fig. 10 shows the calculated power in a normal operating condition and with a frozen leg condition as a function of phase shift. It is assumed that $alpha = 10^o$ and the parameters are: $f = 25\ kHz$, $L = 16\ uH$ and $V_1 = 700\ V$.

IV. VALIDATION OF THE PERFORMED ANALYSIS

To validate the performed analysis, simulations and experiments have been conducted where the results showed an acceptable agreement between these parts which are presented in this section.

Matlab/Plecs simulation tool is used for the simulation. The controller dead-band, a simplified model for the parasitic components such as capacitor series resistors are considered in the simulations. For a input voltage of 537 V, output voltage of 250 V and a phase-shift angle of $\varphi = 8.8\ ^o$ transformer primary currents and the output dc currents are shown in Fig. 8 and Fig. 9 for a normal operation mode and a frozen leg condition, subsequently. The dc output current is reduced from 45.4 A till 43.3 A after the fault. Considering the output voltage, 250 V, the transferred power is reduced from 11.350 kW till 10.825 kW. In addition, the transformer currents are slightly unbalanced after freezing the leg.

A 50 kW experimental setup is constructed for fast charging applications. SiC modules and nanocrystalline magnetic materials are used in the setup. The transformer leakage inductances are used as the energy storage devices and no external inductors are used to achieve more compact size. Fig. 10 shows the constructed setup.

Measurement for a power level of 11.2 kW is shown in Fig. 11. In this case the primary voltage is 537 V and the secondary voltage is 250 V. The converter has a switching frequency of 25 kHz and the equivalent inductance per phase is 16 uH. After a leg halt in the secondary of the converter, the output current is reduced from 44.8 A to 36.8 A. Hence, the output power is reduced to 9.2 kW. The transformer currents in this figure show a slight unbalanced operation mode which is expected from the performed analysis and simulation. For example the peak values of the phase A and C are 26 A and 24.7 A.

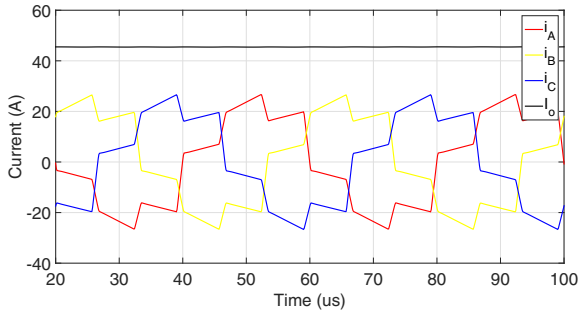

Fig. 8. Simulation results for a normal operation condition.

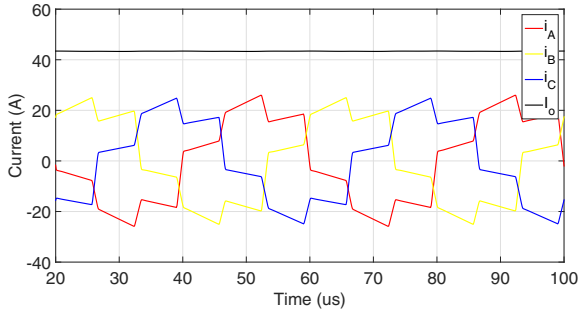

Fig. 9. Simulation results after a frozen leg.

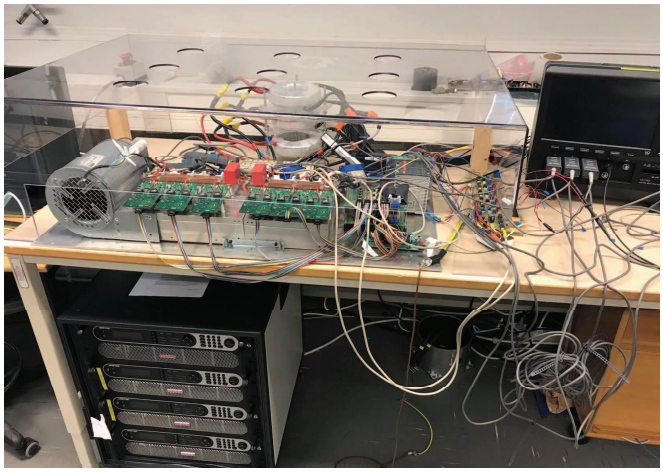

Fig. 10. The constructed 50 kW three-phase DAB converter.

V. FAULT DETECTION AND POST-FAULT STRATEGY

For a three-phase DAB converter, the input/output voltages are measured and used in the control system to adjust the phase-shift for the power control. In addition, it is common to measure the output current for protection or control. Hence, it is possible to check that the commanded phase shift is delivering the intended power. If the transferred power is less than expected value calculated in (1), it is concluded that there is a fault in the system. By processing the transformer currents, which is unbalanced in this fault mode, the frozen leg mode can be detected.

If a frozen leg mode is detected, it is possible to restart the normal operation by inserting a physical reset signal to the driver. In this case, auxiliary circuits are needed to add this functionality to the system.

As it is shown in this work, a frozen leg case is a non-destructive fault mode. It means that if the components can tolerate extra stress, it is possible to continue the operation in an unbalanced mode. The thermal system would be sized for the total losses and it is able to handle this fault mode. Consequently, power modules should be oversized to be able to continue the operation, too.

As a recommendation in the design change and post-fault strategy, it is desirable to have power semiconductors with some extra margins in order to be able to increase the reference values to achieve the nominal power level.

VI. CONCLUSION

A frozen leg condition of a three-phase DAB converter at light loads is considered in this paper. Performed analysis, simulations and experiments show that this fault mode is non-destructive. However, the power transfer capability is reduced which analytical formula is provided to quantify this performance degradation. By over sizing the electronic components and some consideration in the controller, it is possible to continue the operation while waiting a maintenance action.

ACKNOWLEDGMENT

The authors would like to thank the Swedish Energy Agency and Elbind Elektronik AB for financial support of the project.

REFERENCES

[1] A. Kuperman, U. Levy, J. Goren, A. Zafransky and A. Savernin, "Battery Charger for Electric Vehicle Traction Battery Switch Station," in IEEE Transactions on Industrial Electronics, vol. 60, no. 12, pp. 5391-5399, Dec. 2013.

[2] S. Haghbin, "Design considerations of a 50 kW compact fast charger stations using nanocrystalline magnetic materials and SiC modules," 2016 Eleventh International Conference on Ecological Vehicles and Renewable Energies (EVER), Monte Carlo, 2016, pp. 1-6.

[3] H. S. H. Wang, F. Blaabjerg and M. Pecht, Reliability of Power Electronic Converter Systems, IET, 2015, ISBN: 978-1-84919-901-8.

[4] R. W. A. A. De Doncker, D. M. Divan and M. H. Kheraluwala, "A three-phase soft-switched high-power-density DC-DC converter for high-power applications," in IEEE Transactions on Industry Applications, vol. 27, no. 1, pp. 63-73, Jan/Feb 1991.

[5] F. Krismer and J. W. Kolar, "Efficiency-Optimized High-Current Dual Active Bridge Converter for Automotive Applications," in IEEE Transactions on Industrial Electronics, vol. 59, no. 7, pp. 2745-2760, July 2012.

[6] B. Zhao, Q. Song, W. Liu and Y. Sun, "Overview of Dual-Active-Bridge Isolated Bidirectional DC/DC Connverter for High Fequency Link Power Conversion System," in IEEE Transactions on Power Electronics, vol. 29, no. 8, pp. 4091-4106, Aug. 2014.

[7] S. P. Engel, N. Soltau, H. Stagge and R. W. De Doncker, "Dynamic and Balanced Control of Three-Phase High-Power Dual-Active Bridge DC-DC Converters in DC-Grid Applications," in IEEE Transactions on Power Electronics, vol. 28, no. 4, pp. 1880-1889, April 2013.

[8] S. Haghbin, "Electrical failure mode and effect analysis of a 3.3 kW onboard vehicle battery charger," 2016 18th European Conference on Power Electronics and Applications (EPE'16 ECCE Europe), Karlsruhe, 2016, pp. 1-10.

[9] Y. Song and B. Wang, "Survey on Reliability of Power Electronic Systems," in IEEE Transactions on Power Electronics, vol. 28, no. 1, pp. 591-604, Jan. 2013.

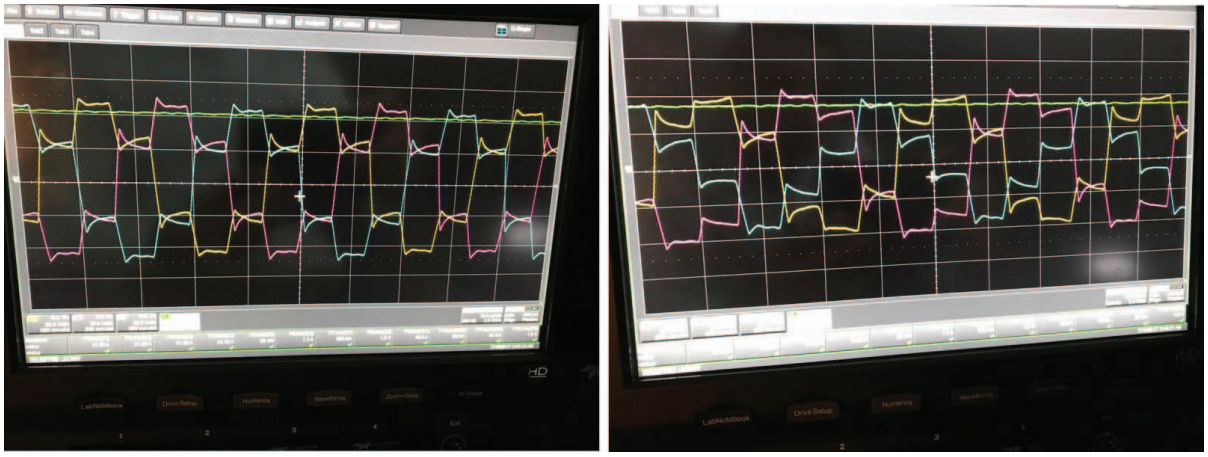

Fig. 11. The measurement results in a normal mode (left) and after the frozen leg (right).

[10] W. Zhang, D. Xu, P. N. Enjeti, H. Li, J. T. Hawke and H. S. Krishnamoorthy, "Survey on Fault-Tolerant Techniques for Power Electronic Converters," in IEEE Transactions on Power Electronics, vol. 29, no. 12, pp. 6319-6331, Dec. 2014.

[11] R. Bono, R. Alexander, A. Dorman, Yong-Jin Kim and J. Reisdorf, "Analyzing reliability - a simple yet rigorous approach," in IEEE Transactions on Industry Applications, vol. 40, no. 4, pp. 950-957, July-Aug. 2004.

[12] U. M. Choi, F. Blaabjerg and S. Jorgensen, "Power Cycling Test Methods for Reliability Assessment of Power Device Modules in respect to Temperature Stress," in IEEE Transactions on Power Electronics, DOI 10.1109/TPEL.2017.2690500, 2017.

[13] A. K. Tripathi, K. Hatua and S. Bhattacharya, "A comparative study of three-phase dual active bridge topologies and their suitability for D-Q mode control," 2012 IEEE Energy Conversion Congress and Exposition (ECCE), Raleigh, NC, 2012, pp. 1719-1724.

[14] N. H. Baars, J. Everts, H. Huisman, J. L. Duarte and E. A. Lomonova, "A 80-kW Isolated DC-DC Converter for Railway Applications," in IEEE Transactions on Power Electronics, vol. 30, no. 12, pp. 6639-6647, Dec. 2015.

[15] Z. Qin, Y. Shen, P. C. Loh, H. Wang and F. Blaabjerg, "A Dual Active Bridge Converter with an Extended High-Efficiency Range by DC Blocking Capacitor Voltage Control," in IEEE Transactions on Power Electronics, vol. PP, no. 99, pp. 1-1.